Structure and Dynamics of Shock-Induced Nanobubble Collapse in Water

M. Vedadi, A. Choubey, K. Nomura, R. K. Kalia,* A. Nakano, and P. Vashishta
Collaboratory for Advanced Computing and Simulations, University of Southern California, Los Angeles, California 90089-0242, USA

A. C. T. van Duin
Department of Mechanical and Nuclear Engineering, Pennsylvania State University, University Park, Pennsylvania 16802, USA
(Received 8 October 2009; revised manuscript received 1 April 2010; published 1 July 2010)

Shock-induced collapse of nanobubbles in water is investigated with molecular dynamics simulations based on a reactive force field. We observe a focused jet at the onset of bubble shrinkage and a secondary shock wave upon bubble collapse. The jet length scales linearly with the nanobubble radius, as observed in experiments on micron-to-millimeter size bubbles. Shock induces dramatic structural changes, including an ice-VII-like structural motif at a particle velocity of 1 km/s. The incipient ice VII formation and the calculated Hugoniot curve are in good agreement with experimental results.

DOI: 10.1103/PhysRevLett.105.014503 PACS numbers: 47.55.dd, 47.11.−j, 47.40.−x

When a bubble interacts with a shock wave, it collapses because the surface tension cannot provide enough restoring force. Experimental studies on micron-size bubbles reveal that the impact of a pulsed shock on the proximal side of the bubble shrinks and accelerates it in the direction of the shock propagation. Furthermore, the liquid around the collapsing bubble forms a jet which creates a protrusion and secondary water hammer shock wave when it hits the distal side of the bubble and breaks up [1]. The behavior of a collapsing bubble depends on its location relative to objects embedded in the fluid as well as the shock wave characteristics (amplitude and pulse width) and the initial size of the bubble. Shock-induced bubble collapse phenomena have been studied in the context of a single bubble [2–4] as well as multiple bubbles [5] near a rigid boundary and in confined environments (e.g., microfluidic or lab-on-a-chip systems) [6,7].

Jetting and secondary water hammer shocks can cause significant damage in materials. This problem is encountered in the disintegration of blades of ship propellers, pipelines, and pump blades [8]. In medicine, however, collapsing bubbles have found useful applications such as extracorporeal shock wave lithotripsy [9] and targeted drug delivery [10]. In the so-called sonoporation approach, the collapse of microbubbles generates liquid jets and radial spreading flows [11] that can make the cell membrane transiently permeable to molecular entry. This has potential applications in gene therapy and anticancer drug delivery [12,13].

In this Letter, we report molecular dynamics (MD) simulations of shock-induced collapse of nanobubbles in water. The MD approach is well suited to study this problem because it can provide direct information about the structure and dynamics of nanobubble collapse over microscopic spatiotemporal scales. Contained in this microscopic information are some of the subtle but salient features of bubble collapse that experiments or continuum simulations may not be able to capture.

The MD simulations reported here are based on quantum-mechanically informed reactive force fields (ReaxFF), which can accurately describe bond breaking or formation and chemical reactions in the system [14,15]. Using a scalable fast reactive force field algorithm (F-ReaxFF) [16,17], we have performed MD simulations of water subjected to planar shock with and without a nanobubble. The initial volume of the MD box is $38.5 \times 18.6 \times 16.6$ nm^3 and the system contains $N = 10^6$ atoms. We equilibrate the system in the (N, V, T) ensemble with periodic boundary condition in all directions. The initial mass density and temperature are 0.98 g/cc and $T = 300$ K, respectively. After equilibration, we insert nanobubbles of diameters $D = 6$, 8, and 10 nm at the center of the MD cell by removing 90% of water molecules from the nanobubble spheres; see Fig. S1 (in the supplementary material [18]) [19].

These equilibrated systems are then subjected to planar shocks with particle velocities $u_p = 1.0$, 2.5, 3.0, or 3.5 km/s using a momentum mirror (see the inset in Fig. 1). In shock simulations we insert a 2-nm-thick vacuum layer at the end of the MD cell in the x direction (shock direction), turn off the thermostat coupling, and apply periodic boundary conditions in lateral directions to minimize surface effects normal to the shock direction. The distance between a nanobubble and its nearest mirror image (≥ 6.6 nm) is much larger than the cutoff length (1 nm) of ReaxFF, which rules out any interaction between the bubble and its images. The integration time step in these MD simulations is 0.1 fsec.

We first performed shock simulations without the nanobubble to validate the ReaxFF for water. Figure 1 shows the MD (red circles) and experimental (blue crosses) [20] results for the shock velocity u_s versus u_p, i.e., the

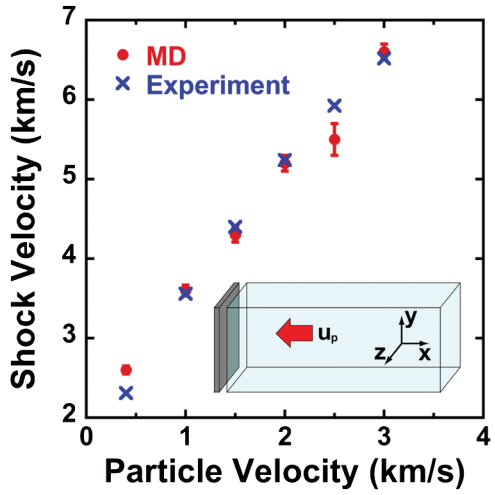

FIG. 1 (color). Experimental (blue crosses) and MD (red circles) Hugoniot compression curves for u_p between 0.4 and 3 km/s. The inset shows the simulation cell and the momentum mirror (gray plate).

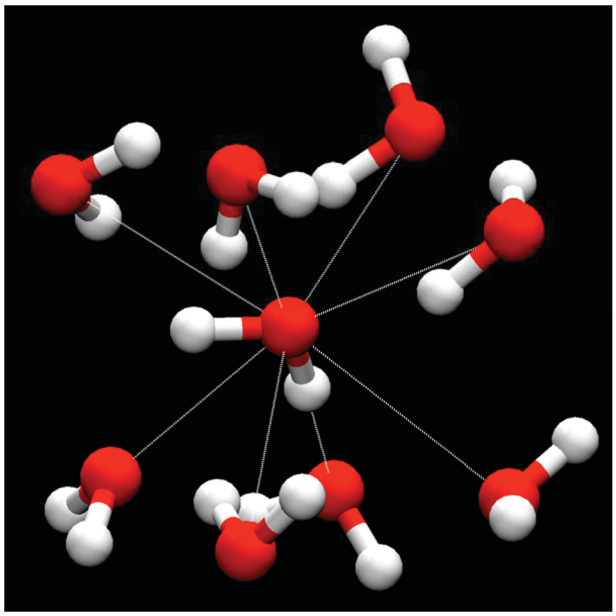

FIG. 2 (color). Snapshot of a water molecule cluster that forms an ice-VII-like structure in the compressed region at $u_p = 1$ km/s. Red spheres and white spheres represent oxygen and hydrogen atoms, respectively. Dotted lines indicate the directions of nearest-neighbor oxygen atoms (within 3 Å from the central oxygen atom).

Hugoniot curve. Shock velocity is obtained from the difference in the shock-front boundaries at two time frames. In each frame, the abrupt change in the density identifies the location of the shock front. The simulation results are in good agreement with the experimental data [20].

Shock produces significant structural changes in water, as shown in Fig. S2 in the supplementary material [18] for the oxygen-oxygen radial distribution function. The most interesting structural changes occur at $u_p = 1$ km/s. In the primary shock region, we find molecular clusters in which a water molecule has eight nearest neighbors in a body-centered-cubic lattice configuration, indicating the nucleation of ice VII; see Fig. 2. In this ice VII structure, the central oxygen atom is connected to four of its nearest-neighbor oxygen atoms through hydrogen bonds [21,22]. We do not find an icelike structure at other particle velocities ($u_p = 2.5$, 3.0, and 3.5 km/s), which is in agreement with experimental observations of ice VII only for particle velocities between 0.75 and 2 km/s [20].

Figure 3(a) shows shock-induced changes in the bubble volume (normalized by the initial bubble volume) and shape of the bubble for $D = 10$ nm. The insets show oxygen atoms of water molecules at the periphery of the nanobubble before the shock wave strikes the nanobubble and just before the nanobubble collapses. The volume versus time data correspond to bubble diameters $D = 6$, 8, and 10 nm and particle velocity $u_p = 3$ km/s. The bubble collapse time τ is estimated to be 1.1, 1.4, and 1.7 ps for $D = 6$, 8, and 10 nm, respectively. According to the Rayleigh formula ($\tau = 0.45D\sqrt{\frac{\rho}{\Delta P}}$, where ρ is the mass density and ΔP is the pressure difference across the bubble surface), τ for the three bubble sizes is 0.8, 1.1, and 1.4 ps. The differences between the MD results and Rayleigh formula arise for the following reasons: (1) in Rayleigh collapse it is assumed that the bubble is within a uniform fluid, whereas the pressure and density around the nanobubble become nonuniform when the shock front reaches the nanobubble, and (2) unlike MD simulations, the Rayleigh equation does not include viscosity and surface tension effects arising from interatomic interactions. It should be pointed out that we are dealing with cavitation nanobubbles which collapse under large compression (see Fig. S3 in the supplementary material [18]), whereas surface gas nanobubbles under small tension or compression (6 MPa) are experimentally found to be stable [23].

Figures 3(b) and 3(c) show velocity profiles of water molecules around a shrinking nanobubble ($D = 10$ nm) at $u_p = 3$ km/s. At $t = 3.3$ ps the nanobubble has shrunk significantly but not collapsed completely under shock compression. The snapshot in Fig. 3(c) is taken immediately after the nanobubble collapses ($t = 3.9$ ps). Here, contours of the magnitude of velocity are color-coded and each arrow represents the direction and the arrow color the magnitude of the average molecular velocity (averaged over all molecules in a voxel of length 0.5 nm) at that position. Regions inside the white dashed lines are enlarged in the insets, and the white arrows indicate the direction of shock propagation. We observe that water molecules around the top and bottom of the nanobubble change directions and their average molecular velocities point towards the center of the bubble soon after the shock wave reaches the proximal side of the bubble. This focusing feature of high-speed molecules from the onset of shrinkage to complete collapse of a nanobubble is akin to the jetting phenomenon observed experimentally in micro-

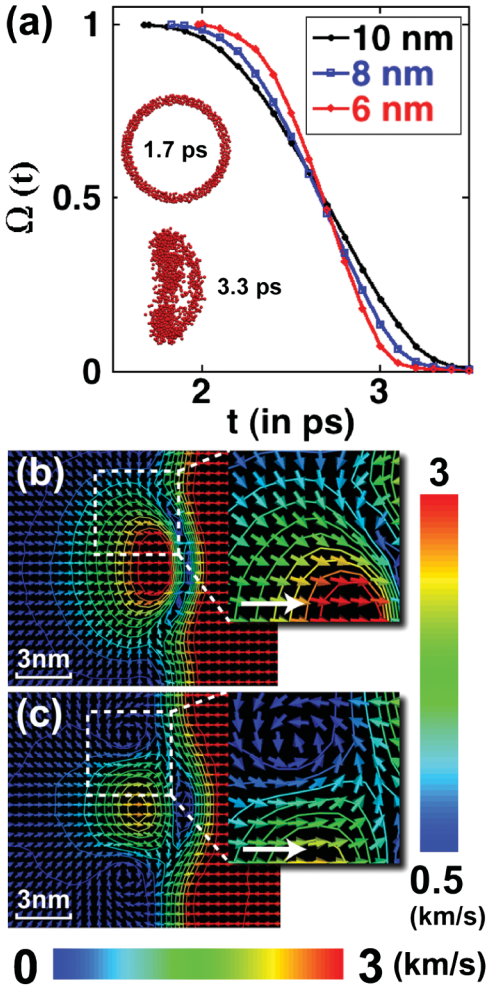

FIG. 3 (color). (a) Normalized bubble volume $\Omega(t)$ versus time t for $D = 6$, 8, and 10 nm. Insets show the bubble shapes before the shock wave strikes and before the nanobubble collapses. Panels (b) and (c) show velocity vector fields in a cross section of the system just before ($t = 3.3$ ps) and soon after ($t = 3.9$ ps) the largest nanobubble collapses. In (b) the region inside the white dashed lines is enlarged to show a focused jet; in (c) the enlarged region shows lateral flow with the onset of jet disintegration.

bubble collapse. The difference between our simulation and experiment [1] is that nanojets do not elongate as much as microjets do beyond the distal side of collapsed bubbles. The formation of nanojets has also been reported in a MD simulation of pressurized fluid injection through a nanoscale nozzle [24]. Figure 3(c) shows molecular motion around the collapsed nanobubble and lateral flow at the periphery of the collapsed region. The lateral flow is smaller than that observed in the vicinity of a solid surface or a lipid bilayer [11,25].

At the onset of nanobubble collapse, we observe a sudden increase in the translational kinetic energy and rotational energy of molecules at the shock front. In the final stages of nanobubble collapse, the molecular vibrational energy also increases to about 0.2 eV (for $u_p = 3$ km/s and $D = 10$ nm), which is well below the self-dissociation energy $[2H_2O \rightarrow OH^- + H_3O^+]$ in pure water.

Figure 4 shows the effects of u_p and D on velocity vector fields of water molecules in and around the nanobubble just after it collapses. Figures 4(a)–4(c) show that the size of the jet (ellipsoidal red region) increases with an increase in D. Figures 4(d)–4(f) show the effect of u_p on the molecular velocity vector fields in systems containing a nanobubble with $D = 10$ nm. The high-speed region does not grow as much with an increase in the particle velocity as with the nanobubble size.

From the onset of nanojet formation and disintegration, we have determined the penetration length l_{jet} and persistence time τ_{jet} for the jet. For all particle velocities we find l_{jet} increases linearly with D [26]. This has also been observed in experiments on micron-to-millimeter size bubbles [1,27]. This agreement is somewhat surprising because viscosity and surface tension may play larger roles in nanobubbles than in micron-to-millimeter size bubbles. We find the nanojet persistence time is longer than the nanobubble collapse time by about 0.2 ps. Also, the nanojet velocity, $V_{\text{jet}} = l_{\text{jet}}/\tau_{\text{jet}}$, is higher than u_s, and V_{jet} increases with an increase in the bubble size.

Figure 5 shows the local pressure calculated from the virial expression [28] for $D = 10$ nm at $u_p = 3$ km/s. The pressure in the compressed region remains constant and the wave front remains planar until the shock wave reaches the nanobubble; see Fig. 5(a). The pressure (18.8 GPa) is in reasonable accord with the estimate (19.5 GPa) from the jump condition, $p - p_0 = \rho_0 u_s u_p$ [29]. Figure 5(b) shows a concave wave front due to pressure gradient during the nanobubble collapse. The shock front becomes planar again just before the complete collapse of the nanobubble; see Fig. 5(c). When the primary shock wave hits the proximal side of the nanobubble, surrounding water molecules move into the nanobubble with high speeds. On reaching the distal side of the nanobubble, these high-

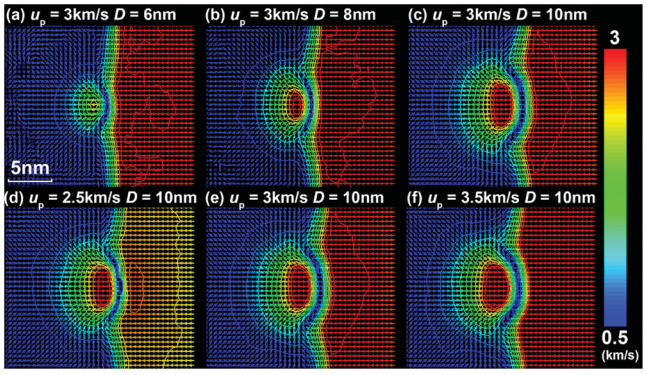

FIG. 4 (color). Effects of particle velocity and nanobubble size on bubble collapse. Snapshots (a)–(c) are taken for $u_p = 3$ km/s and $D = 6$, 8, and 10 nm, respectively. Snapshots (d)–(f) are for $D = 10$ nm and $u_p = 2.5$, 3.0, and 3.5 km/s, respectively. The size of the high-speed region (ellipsoidal red regions) increases more with an increase in D than with u_p.

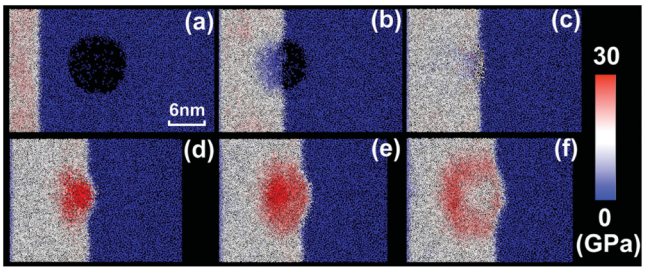

FIG. 5 (color). Panel (a)–(c) show the primary shock wave at $t = 1.6$, 2.9, and 3.3 ps, respectively. Here, $u_p = 3$ km/s and $D = 10$ nm. Panels (d)–(f) show the secondary water hammer shock at $t = 3.5$, 3.7, and 3.9 ps, respectively. The color code corresponds to pressure.

speed molecules give rise to a secondary water hammer shock wave with a maximum pressure of 29 GPa [Fig. 5(d)]. The water hammer shock propagates backward (opposite to the primary shock), spreading spherically with a velocity of 8 km/s as the pressure decreases; see Figs. 5(e) and 5(f) [30]. Significant pressure amplification due to secondary water hammer shock wave and its rapid dissipation have also been observed in experiments [2] and continuum simulations [31].

In conclusion, the F-ReaxFF MD simulations of shock propagation in water are in good agreement with experimental results for the Hugoniot compression curve. We find molecular clusters with ice-VII-like structure at particle velocity of 1 km/s. This is well supported by experimental observations of ice VII for particle velocities between 0.75 and 2 km/s. We have examined the effects of shock amplitude and the initial nanobubble size on the dynamics of nanobubble shrinkage and collapse. During shrinkage, we observe a focused nanojet whose length scales linearly with the nanobubble radius. This scaling relation has also been found experimentally in shock-induced collapse of micron-to-millimeter size bubbles. Currently, we are performing multimillion-atom MD simulations to examine the effect of nanojets from nanobubble collapse on lipid bilayers. Our preliminary results indicate that the nanojet impact creates a transient localized deformation of nonuniform width and poration in the lipid bilayer (see the movie and Fig. S4 in the supplementary material [18]). In addition, we observe shear flow of water on the lipid bilayer (see Fig. S5 in the supplementary material [18]) which has also been reported in experiments on the interaction of cavitation bubbles with cells [11]. Transient cell poration has potential applications in gene therapy and drug delivery.

This work was supported by DOE-BES, DOE-SciDAC, NSF-ITR, and NSF-PetaApps grants. Simulations were performed at USC's High Performance Computing Facility and on our cluster in the Collaboratory for Advanced Computing and Simulations.

*To whom correspondence should be addressed.
rkalia@usc.edu

[1] C. D. Ohl and R. Ikink, Phys. Rev. Lett. **90**, 214502 (2003).
[2] E. A. Brujan *et al.*, Phys. Fluids **14**, 85 (2002).
[3] Y. Tomita and T. Kodama, J. Appl. Phys. **94**, 2809 (2003).
[4] G. N. Sankin and P. Zhong, Phys. Rev. E **74**, 046304 (2006).
[5] A. Tufaile and J. C. Sartorelli, Phys. Rev. E **66**, 056204 (2002).
[6] E. Zwaan *et al.*, Phys. Rev. Lett. **98**, 254501 (2007).
[7] V. S. Ajaev and G. M. Homsy, Annu. Rev. Fluid Mech. **38**, 277 (2006).
[8] C. E. Brennen, *Cavitation and Bubble Dynamics* (Oxford University Press, New York, 1995), p. 282.
[9] T. Kodama and K. Takayama, Ultrasound Med. Biol. **24**, 723 (1998).
[10] T. Kodama, M. R. Hamblin, and A. G. Doukas, Biophys. J. **79**, 1821 (2000).
[11] C. D. Ohl *et al.*, Appl. Phys. Lett. **89**, 074102 (2006).
[12] M. Delius and G. Adams, Cancer Res. **59**, 5227 (1999).
[13] T. Kodama *et al.*, J. Biomech. Sci. Eng. **4**, 124 (2009).
[14] A. C. T. van Duin *et al.*, J. Phys. Chem. A **105**, 9396 (2001).
[15] In ReaxFF MD simulations, we find no chemical reactions during the nanobubble collapse. Consequently, MD simulations with simpler force fields (e.g., simple point charge) for water may also capture the nanojet phenomenon.
[16] A. Nakano *et al.*, Comput. Mater. Sci. **38**, 642 (2007).
[17] K. Nomura *et al.*, Comput. Phys. Commun. **178**, 73 (2008).
[18] See supplementary material at http://link.aps.org/supplemental/10.1103/PhysRevLett.105.014503 for the description of the reactive force field, the simulation setup, and structural and dynamic correlations of nanobubble collapse.
[19] The nanobubbles are subjected to shock compression so rapidly (~1 ps) that they do not have time to shrink on their own.
[20] A. P. Rybakov and I. A. Rybakov, Eur. J. Mech. B, Fluids **14**, 323 (1995).
[21] J. D. Jorgensen and T. G. Worlton, J. Chem. Phys. **83**, 329 (1985).
[22] S. Klotz *et al.*, Nature Mater. **8**, 405 (2009).
[23] B. M. Borkent *et al.*, Phys. Rev. Lett. **98**, 204502 (2007).
[24] M. Moseler and U. Landman, Science **289**, 1165 (2000).
[25] C. D. Ohl *et al.*, Biophys. J. **91**, 4285 (2006).
[26] For example, we find that l_{jet} increases from 7.8 to 14.7 nm as R increases from 3 to 5 nm.
[27] T. Kodama and Y. Tomita, Appl. Phys. B **70**, 139 (2000).
[28] Z. H. Sun *et al.*, Model. Simul. Mater. Sci. Eng. **14**, 423 (2006).
[29] Z. U. A. Warsi, *Fluid Dynamics: Theoretical and Computational Approaches* (CRC Press, Boca Raton, FL, 1998), p. 752.
[30] Snapshots in Fig. 5 show that the water hammer shock is not close to the lateral boundaries and so the interaction between mirror-image waves is negligible.
[31] E. Johnsen and T. Colonius, J. Acoust. Soc. Am. **124**, 2011 (2008).